



A multi-objective optimization design for a new linear compliant mechanism

Minh Phung Dang¹ · Hieu Giang Le¹ · Ngoc Le Chau² · Thanh-Phong Dao^{3,4}

Received: 8 July 2019 / Revised: 25 September 2019 / Accepted: 25 September 2019 /

Published online: 29 September 2019

© Springer Science+Business Media, LLC, part of Springer Nature 2019

Abstract

This paper develops a hybrid optimization approach for multi-criteria optimal design of a compliant positioning platform for nanoindentation tester. The platform mimics the biomechanical behavior of beetle so as to allow a linear motion. Structure of the beetle-like mechanism consists of six legs arranging in a symmetric topology. Amplification ratio and static characteristics of the platform are analyzed by finite element analysis (FEA). To improve the performances of the platform, the main geometric parameters of the platform are optimized by an efficient hybrid approach of the Taguchi method (TM), response surface methodology (RSM), improved adaptive neuro-fuzzy inference system (ANFIS), and teaching learning based optimization (TLBO). Numerical data are collected by integrating of the RSM and FEA. Signal to noise ratios are determined and the weight factor of each response is calculated. The suitable ANFIS's parameters are optimized through the TM. The results found that trapezoidal-shaped MFs is the best type for the safety factor and the displacement. The optimal ANFIS's parameters for the safety factor and the displacement were determined at the number of input MFs of 4, trapmf, hybrid learning method, and linear output MFs. According to improved ANFIS establishments, TLBO algorithm is utilized for solving the multi-objective optimization. Analysis of variance and sensitivity are investigated to determine the significant effects of design factors on the responses. The simulated and experimental validations are in a good agreement with the predicted results.

Keywords Compliant positioning platform · Multi-objective optimization · Taguchi method · Response surface method · Adaptive neuro-fuzzy inference system · TLBO · Weight factor

✉ Thanh-Phong Dao
daothanhphong@tdtu.edu.vn

Extended author information available on the last page of the article

1 Introduction

Nanoindentation tester is designed for the measurement of hardness, elastic modulus and creep. The system can be adopted to define characteristics of organic, inorganic, hard and soft materials. An indentation measurement can be carried out in less than 3 min without waiting for thermal stabilization with the unique top surface referencing technique. Therefore, a positioning process has to be high precisely. Materials can be checked, including hard and soft types from tissue, biological cell, semiconductor nanomaterial, optics, material science, biomechanics, micro-electro-mechanical systems, and electronics (Hu et al. 2013; O'Brien et al. 2005; Nohava et al. 2009). During the indentation process, multiple microscopes are used to record the image of sample before and after indenting test to characterize the curve of displacement versus load while a material sample is bring to in front of microscope. In order to obtain a good image quality, a precise positioning platform is essential to locate the sample material. It means that the positioning platform is an important mechanism for the nanoindentation system. In commercialization, the entire system is difficult to gain high position accuracy due to using servo motors, ball screws, and rigid joint. This leads unfavorable disadvantages such as backlash, friction, and wear. To overcome the disadvantages of traditional technologies, a compliant positioning platform is proposed to improve the resolution of system because of essential merits such as no wear, no backlash, free friction, monolithic structure, light weight, low cost, no lubricant, high precision and compact structure (Xu 2014; Lu et al. 2014; Dao et al. 2017a, b; Polit and Dong 2011; Song et al. 2010; Dao et al. 2017a, b; Fung and Lin 2009). Similar to different applications, the indentation system also requires a large working travel with a high safety factor in order to conduct various positioning tasks.

A few recent years, regarding a large working travel, many studies have been conducted. Some concentrated on the use of various amplifiers (Ling et al. 2016). A large working travel of positioning stages were designed (Dao et al. 2017a, b). Yong et al. (2009) developed the amplification levers for a fast nanoscale positioning. Kang et al. (2005) proposed displacement amplification mechanism integrated platform-type parallel mechanisms using flexure hinges. Kim et al. (2012) utilized a double displacement amplifier for a 3-DOFs positioning system. Xu and Li (2011) presented an optimization of an integration bridge amplification mechanism. Le Zhu et al. (2018) designed an amplifier integrated a Scott-Russell mechanism and a half-bridge mechanism for 2DOFs nanopositioning stage. Unlike previous studies, inspired from a high flexibility in beetle's motion, the proposed platform is designed so as to reach a small parasitic motion. Subsequently, a new multi-lever displacement amplifier is integrated inside the platform so as to generate a large working stroke. However, the platform is difficult to obtain a large displacement and ensure a good strength, simultaneously through a design process. As known, two quality responses are conflicted together. Therefore, a multi-objective optimization problem is needed to balance between them.

Regarding an multi-objective optimization process, Huang and Dao (2016a, b) optimized a compliant XY positioning stage utilizing the finite element analysis

(FEA) and response surface methodology (RSM). Xiao et al. (2011) optimized the stiffness, working travel and safety factor using the radius basis functional network combined genetic algorithm. More recent years, Dao et al. (2017a, b) developed a hybrid Taguchi-cuckoo search algorithm to optimize overall the quality responses, simultaneously for a flexure-based focus locating stage. A hybrid approach of the grey relational analysis, Taguchi, RSM and entropy measurement was combined (Huang and Dao 2016a, b). RSM was integrated with the GA (Álvarez et al. 2009; Bahloul et al. 2013), ANFIS and Jaya (Suraj et al. 2016), GA and ant colony optimization (Zukhri and Papatungan 2013). In addition, Ling et al. (2019) proposed a kinematics-based optimization method for 2-DOF millimeter-range monolithic flexure mechanism. Generally, population-based optimization algorithms often require initially controllable parameters while the teaching learning based optimization (TLBO) could optimize rapidly multi-criteria with less parameters. So, the TLBO is proposed to conduct multi-objective optimization problem for the proposed platform. Prior to implement the TLBO programming, the mathematical equations or surrogate models for both displacement and safety factor should be established well. Because the compliant platform is a non-traditional type of mechanical engineering, the mathematical models are complicated to be established. If these equations may be wrong, the further optimized solutions are not true.

For a real compliant positioning platform, a good relation between design variables and quality responses are difficult to establish precise equations. Therefore, it leads an imprecisely optimized solution. As known, the RSM is considered as a surrogate model and can approximate a regression model but the prediction accuracy of the RSM is strongly dependent on the coefficient of determination. To cover come this limitation, artificial intelligences have been developed for various fields in which adaptive neuro-fuzzy inference system (ANFIS) is one of the most effective approaches. ANFIS is considered as an effective black box via an integration of fuzzy logic and neural network (Wei 2016; Cheng and Wei 2009). So, ANFIS is further adopted for the proposed platform. Even though the ANFIS is still useful for various problems but a basic ANFIS structure are largely dependent following four main controllable parameters as: (1) the number of input membership functions (MFs) of the fuzzy logic, (2) types of input MFs, (3) the training method such as hybrid procedure or back propagation, and (4) type of output MFs. However, most previous studies used these parameters as default and there have no considerations in identifying the suitable parameters of the ANFIS structure for a specific problem. In order to determine the appropriate parameters for ANFIS, the Taguchi method (TM) is utilized to optimize the root mean squared error, which is a performance metric of ANFIS. Based on the optimized parameters of ANFIS, a surrogate model is well established for the platform. In addition, for a multi-objective optimization problem, the weight factor (WF) for each response is different. The WF is often chosen based on the experiences or customer's demands. Unlike previous studies, the WF can determined exactly via establishing the set of statistical equations because the WF depends on the sensitivity of design variables to responses.

The main aims of this study is to develop a new integration approach to conduct a multi-criteria optimization design for the beetle-inspired platform. A multi-lever

displacement is designed to amplify the working travel. Sensitivity of design variables is analysed. The optimization principle consists of the following phases. First of all, the numerical data are collected by integrating FEA and RSM. Next, the WFs are computed accurately based on statistical equations. And then, the suitable controllable elements for a ANFIS structure is optimized by the TM. After improving the ANFIS structure, the relationships between the design variables and quality objectives are mapped by the improved ANFIS model. Finally, TLBO algorithm is adopted for solving the multi-objective optimization. A prototype was fabricated and its behaviors are tested to verify the predicted results.

2 Conceptual design

2.1 Compliant positioning platform

Inspired from the beetle's movement, a new compliant positioning platform (CPP) was designed so as to reach the linear output displacement as well as decline parasitic motion, as depicted as Fig. 1a, b. Moreover, the body and leg movements of beetles are almost quite in the same plane and the high flexibility of their legs. Hence, beetle-like mechanism is suitable to construct a planar motion mechanism. Figure 1a is an image of a real beetle. Based on the shape of each beetle leg, one of its legs can be proposed to divide into five sections. This geometry can be imitated to develop a mechanism for a linear motion generation. Therefore, a model of the proposed CPP with five segments was designed, as shown in Fig. 1b. It included rigid links and flexure hinges. Its motion was replied on the flexure hinges. As a result, the geometric parameters of flexure hinges contributes largely on the performances of the CPP.

The beetle-liked mechanism ensures a linear motion along the vertical direction and suppresses a parasitic motion along the horizontal direction. Overall performances of the CPP was assessed regarding a large displacement, a small parasitic motion and a high safety factor. A small parasitic motion could achieve by a direct

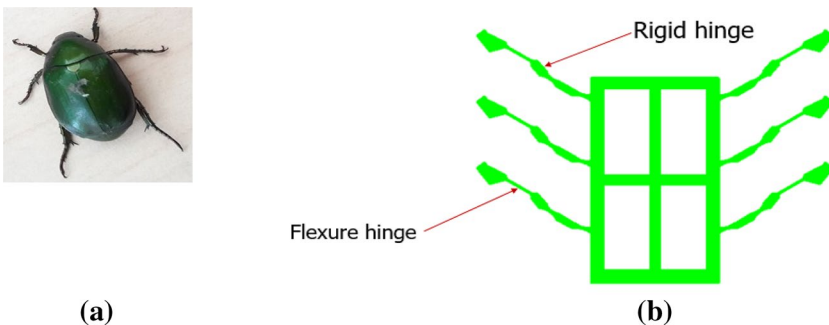


Fig. 1 Model of beetle-inspired platform: **a** beetle animal, **b** compliant positioning platform

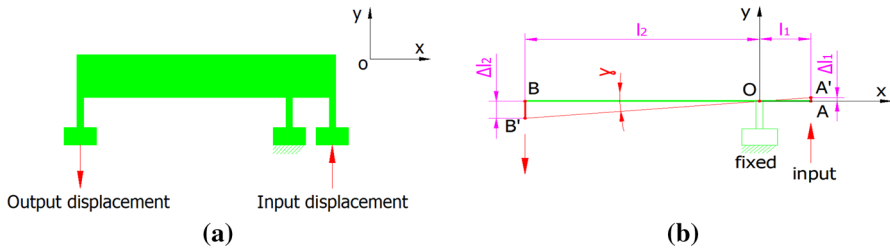


Fig. 2 Diagram: **a** operation principle of lever mechanism, **b** amplification ratio

design but two remain responses have to carry out a further multi-objective optimization problem.

2.2 Displacement amplification mechanism

Traditionally, a lever mechanism is used to amplify the value of force or displacement. Structure of the lever includes of a beam or rigid rod placed on a fixed hinge, or fulcrum, as illustrated in Fig. 2a. Point O is a fixed hinge that is the rotation center of the lever, point A is the input and point B is the output location. The operation principle of lever mechanism is illustrated as follows: when locating a vertical displacement Δl_1 on the input point A, the lever will rotate an angle γ relative to the z-axis. As a result, the point B moves to B' and the output displacement Δl_2 can gain in the vertical direction (y-axis), as illustrated in Fig. 2b. First of all, one lever mechanism can be used to amplify output displacement. However, this mechanism creates easily large parasitic motion. So, a two-lever mechanism was designed to amplify the output displacement and ensure small parasitic motion based on its

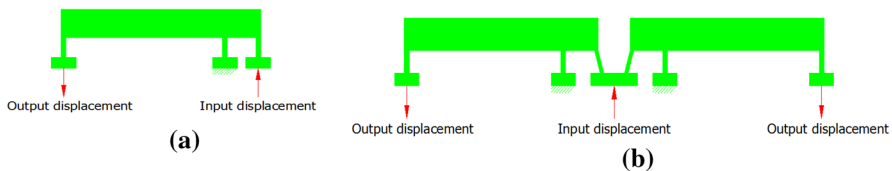
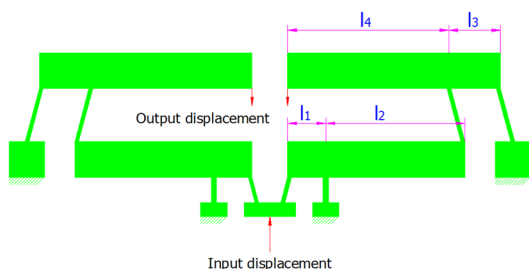


Fig. 3 Model of lever amplifier: **a** one lever mechanism, **b** two lever mechanism

Fig. 4 Model of proposed four-lever displacement amplifier



symmetric structure, as shown in Fig. 3b. Moreover, in order to amplify more large output displacement, four-lever displacement amplifier was proposed in this paper, as depicted in Fig. 4.

Based on a schematic diagram (see in Fig. 2b), the amplification ratio of a lever can be approximately achieved as:

$$r_{lever} = \Delta l_2 / \Delta l_1 = l_2 / l_1 \tag{1}$$

The equation of multi-lever displacement amplifier is assumed as follows:

$$r_T = l_2 / l_1 \times l_4 / l_3 \tag{2}$$

where r_T is amplification ratio of four-lever displacement amplifier.

2.3 Beetle-like platform with amplifier

The operating principle of CPP was based on the elastic deformation of the flexure hinges. In this study, Al T73-7075 was chosen as material for the stage due to its high yield strength of 503 MPa, Young’s modulus of $E=71,700$ MPa, light density of 2810 kg/m^3 and Poisson’s ratio of 0.33. Specification of linear stage was assumed that input displacement was 0.13 mm, as given in Table 1. As seen in Fig. 5, it consisted of elements as follows: (1) twelve fixed holes were utilized to locate the platform on an un-vibration table so as to test its characteristics, (2) a translational screw (locating at the input displacement position) was used to create the input displacement for the platform by connecting directly with the beetle-like mechanism. The total dimension of the model was approximately $230 \text{ mm} \times 222 \text{ mm} \times 6 \text{ mm}$. The geometrical parameters of the platform were given in Table 1. According to a good static performances for positioning system, the proposed platform was required to create a large displacement and a high safety factor, simultaneously.

Based on the design domain and ability of wire electrical discharged machining (WEDM) method as well as designer’s experience, the initial design parameters of the structure were proposed in order to ensure to achieve a high output displacement and be suitable for fabricating by WEDM method. In this study, the geometric

Table 1 Material and structure parameters of the beetle-like platform

Density	Poison’s ratio	Young’s modulus		Yield’s strength	
2810 kg/m^3	0.33	71.70 GPa		503 MPa	
Parameters	Value	Unit	Parameters	Value	Unit
a	6.84	mm	h	$18 \leq h \leq 21$	mm
b	$48 \leq b \leq 53$	mm	t	$0.9 \leq t \leq 1.1$	mm
c	8	mm	m	102	mm
d	30	mm	n	230	mm
e	76	mm	p	222	mm
f	6	mm	q	70	mm
g	5	mm	k	$0.67 \leq k \leq 0.74$	mm

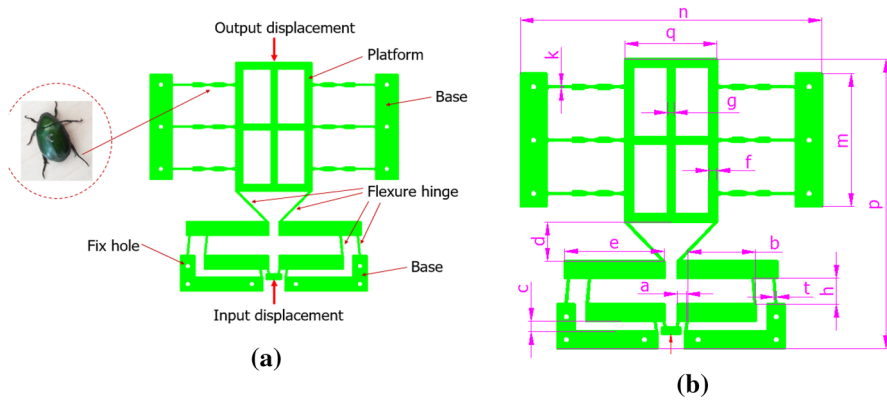


Fig. 5 Model: **a** beetle-like platform, **b** design parameters

parameters (the length and the width as well as radius) of the flexure hinges also affect to the linear motion of the structure. However, compared to other geometric parameters of the beetle leg mechanism, the thickness of flexure hinge is the most significant effect to linear motion and output displacement according to the Euler–Bernoulli beam theory and theory of compliant mechanism. So, this study considered the thickness of flexure hinge of beetle leg mechanism as a main parameter for establishing design variables and ignored the other geometric parameters.

2.4 A basic application for nanoindentation tester

The working principle of proposed CPP was based on the elastic deformation of the material. It was complied with the Hook's law. Therefore, the CPP was operated within the elastic limitation. It was intended to apply in nanoindentation tester. The CPP was utilized for positioning the material sample during nanoindentation testing process. Before indenter translated downward to check the characteristics of the material sample, the CPP would move linearly along the horizontal direction so as to locate the sample to an initially precise position. At the same time, the multiple microscopes were used to take photos of the sample monitoring the initial characteristics of the sample. And then, the indenter would be indented a depth into the testing sample. Next, the CPP would come back a reference position in order to prepare for testing next times. A basic application for nanoindentation tester was proposed in Fig. 6.

3 Analysis of initial performances and parasitic motion error

In this section, a 3D model of platform was designed by Inventor Professional 2018, and then it was simulated via using the finite element analysis in software ANSYS 18.2. The purpose was to forecast the y-axis output displacement and safety factor of

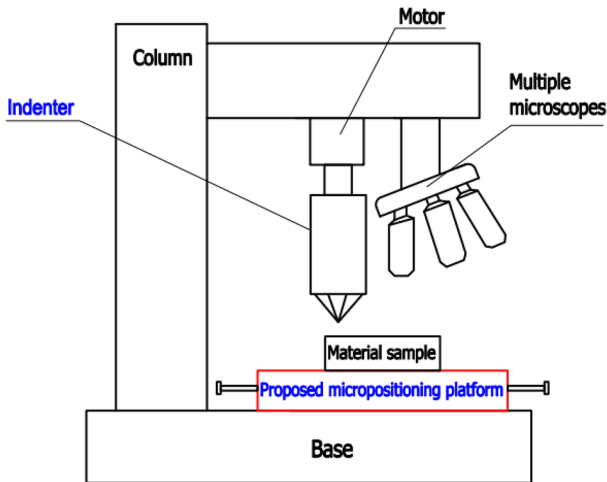


Fig. 6 Nanoindentation testing instrument

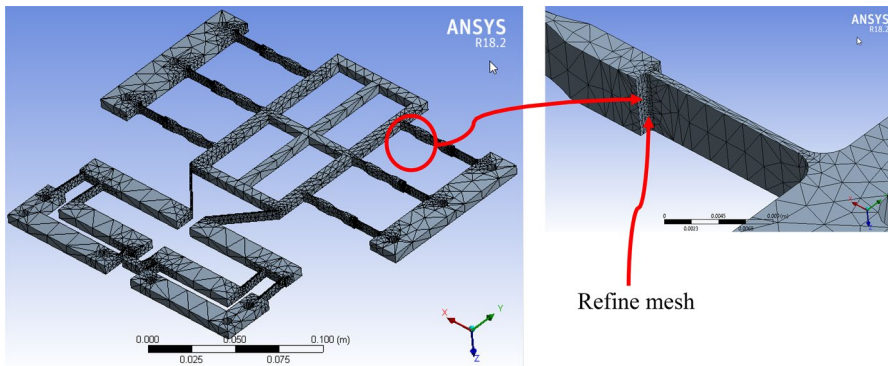


Fig. 7 Mesh generation diagram for the CPP

the CPP. To perform this analysis, the automatic meshing method was applied, and then flexure hinges was refined to achieve a good analysis precision, as illustrated in Fig. 7. The boundary conditions were proposed as follows: the platform was fixed at the holes. After a draft platform was designed, the output displacement of the model was investigated by varying the input displacement of translational screw from 190 to 220 μm , respectively in order to check the limitation of static failure and limit maximal input displacement for initial positioning stage.

In order to check the limitation of plastic deformation failure and determine the range of input displacement for the proposed stage, the input displacement from translational screw was varied from 190 to 220 μm . The corresponding output displacement was recorded. The results of Table 2 found that the output displacement approaches 3.8193 mm with respect to input displacement of 220 μm . This case, the

Table 2 The output displacement

Input displacement (mm)	Output displacement (mm)	Amplification ratio	Safety factor	Von-mises stress (MPa)
0.19	3.2985	17.36	1.1576	434.52
0.2	3.4721	17.36	1.0997	457.39
0.21	3.6457	17.36	1.0473	498.13
0.22	3.8193	17.36	0.99973	503.13

Table 3 Results of output displacement and parasitic error motion

Input displacement (mm)	y-axis output displacement (mm)	x-axis output displacement (mm)	Parasitic error (%)
0.01	0.17361	2.6303e-005	0.01515
0.02	0.34721	5.2606e-005	0.01515
0.03	0.52082	7.8908e-005	0.01515
0.04	0.69442	1.0521e-004	0.01515
0.05	0.86803	1.3151e-004	0.01515
0.06	1.0416	1.5782e-004	0.01515
0.07	1.2152	1.8412e-004	0.01515
0.08	1.3888	2.1042e-004	0.01515
0.09	1.5625	2.3673e-004	0.01515
0.1	1.7361	2.6303e-004	0.01515
0.11	1.9097	2.8933e-004	0.01515
0.12	2.0833	3.1563e-004	0.01515
0.13	2.2569	3.4194e-004	0.01515
0.14	2.4305	3.6824e-004	0.01515
0.15	2.6041	3.9454e-004	0.01515
0.16	2.7777	4.2084e-004	0.01515
0.17	2.9513	4.4715e-004	0.01515
0.18	3.1249	4.7345e-004	0.01515

safety factor was lower than 1 and the resulting stress was about 503.13 MPa which was greater than the critical stress or yield strength of the material (503 MPa), the platform could lead a plastic deformation failure. Therefore, the maximal input displacement should be smaller than 220 μm . Meanwhile, when the input displacement of 190 μm , the resulting stress was approximately 434.52 MPa which was lower than the yield strength of material. The safety factor was about 1.15. In this study, a safety factor over 1.5 was desired so as to ensure a good working life for the platform. As a result, the input displacement was proposed within the range from 10 to 180 μm . By varying the input displacement from 10 to 180 μm , the output displacement in the X-and-Y directions and the parasitic error motion were calculated using Eq. (3). As given in Table 3, the parasitic error motion was relatively small. The results also depicted that the equivalent stress was 297.31 MPa, safety factor was

1.6969, amplification ratio (AR) was 17.3608. However, all results do not meet practical requirements (AR is more than 18). Therefore, an optimization process would be conducted later.

When the platform moved along the y -axis, there was also a motion occurs along the x -axis and at the same time. The undesired movement along the x -axis was called as parasitic motion error. A similar analysis, the numerical simulation results indicated that parasitic motion error is very small with 0.01515% (lower than 1%), as illustrated in Table 3. It could be concluded that the parasitic motion error does not affect significantly to the output displacement accuracy and the proposed platform approaches a good linear movement. The parasitic motion error was defined as follows:

$$e = \frac{x}{y} 100\% \quad (3)$$

where e represents the parasitic error, x and y are the output displacements along the x -axis and y -axis, respectively.

4 Statement of optimization problem

Because the CPP was worked according to elastic deformation of flexure-based joints. As a result, it was affected significantly by geometrical dimensions of flexure-based joints. These dimensions were defined as length of first lever, distance between two levers and thicknesses of flexure hinges. Therefore, in order to enhance the quality responses of the CPP, the main geometrical parameters of the platform should be optimized. The CPP should fulfill the following essential responses as:

- a. A small parasitic motion to increase the accuracy in linear motion;
- b. A large output displacement to expand broad positioning capacity of the platform for checking characteristics of material sample;
- c. A high safety factor to ensure long life of the platform.

A small parasitic error could be achieved via a good design of structure, as described in Sect. 3. However, the displacement and safety factor were difficult to satisfy through a design process. So, it should be enhanced through a further optimization. As known, the safety factor was conflicted with the output displacement. Therefore, so as to trade-off them simultaneously, a new efficient hybrid approach was developed in this study.

4.1 Design variables

Through a few FEA simulations to check initial characteristics, the result showed that the geometric dimensions of flexure hinges were significantly contributed to the displacement and safety factor. In this research, four design variables were considered, consisting of the length of first lever, distance between two levers as well as thicknesses of flexure hinges. The vector of design variables was described as $\mathbf{X} = [t, h, b, k]^T$. The

limit conditions for the design variables were established based on specialized knowledge and design engineer’s professional skills, which were expressed by:

$$\begin{aligned}
 48 \text{ mm} &\leq b \leq 53 \text{ mm} \\
 19 \text{ mm} &\leq h \leq 22.5 \text{ mm}, \\
 0.9 \text{ mm} &\leq t \leq 1.1 \text{ mm} \\
 0.67 \text{ mm} &\leq k \leq 0.74 \text{ mm}
 \end{aligned}
 \tag{4}$$

where t, h, b, k are thickness of flexure hinge (amplification mechanism), distance between two levers, the length of first lever, thickness of flexure hinge (beetle’s leg mechanism), respectively.

4.2 Objective functions

The following multiple-criteria functions were considered: (1) the first objective function, $y_1(\mathbf{X})$, the high safety factor is required to ensure the strength of the platform, requested as high as possible. (2) The second objective function, $y_2(\mathbf{X})$, the output displacement along the y-axis, desired as large as possible in order to expand working travel capacity of the platform for checking characteristics of material sample. In conclusion, the optimization trouble was depicted as follows.

Design variables was regarded as $\mathbf{X} = [t, h, b, k]^T$.

$$\text{Max } y_1(\mathbf{X}) \tag{5}$$

$$\text{Max } y_2(\mathbf{X}) \tag{6}$$

In order to conduct the multi-criteria optimal problem, two objective responses are conveyed into a single criterion function. Then, two objective functions were multiplied with a weight factor. The integrated objective function was declared as follows:

$$y(\mathbf{X}) = -w_1 \times y_1(\mathbf{X}) - w_2 \times y_2(\mathbf{X}), \tag{7}$$

where w_1 and w_2 are the weight factors of two quality responses, respectively.

4.3 Constraints

The proposed platform was operating in a elastic bound of proposed material, it was required to limitations by:

$$g(x) = \sigma \leq \frac{\sigma_y}{SF}, \tag{8}$$

where σ_y is the yield strength of proposed material; and SF is the safety factor.

The safety factor was expected to larger than 1.5 as: on the established

$$y_1(\mathbf{X}) \geq 1.5. \tag{9}$$

The output displacement was desired to more than 2.3 mm as:

$$y_2(\mathbf{X}) \geq 2.3 \text{ mm} \quad (10)$$

where y_1 and y_2 represent the safety factor and displacement, respectively.

5 Proposed hybrid approach

Considering to solve the multi-criteria optimization problem as mentioned, an effective hybrid approach of the RSM, the TM, improved ANFIS and TLBO was developed. Firstly, the experimental data was collected by RSM. Later on, the improved ANFIS was utilized to define relationship between design variables and quality responses. The improved ANFIS was achieved by using the TM. Based on minimization of the RSME, the TM was used to seek the suitable controllable parameters for ANFIS structure. Those parameters included as: (1) the number of input membership functions (MFs) of the fuzzy logic, (2) types of input MFs, (3) the training method such as hybrid procedure or backpropagation, and (4) type of output MFs. Details about ANFIS, the readers can refer to (Cheng and Wei 2009; Linh and Dao 2018; Chau et al. 2018). Finally, based on the established surrogate model from the improved ANFIS, TLBO algorithm was adopted to conduct multi-criteria optimization, simultaneously. The programming was implemented in Matlab R2017. A flowchart for optimal process of the CPP was illustrated in Fig. 8. The optimization process is divided into key phases as follows:

Phase 1: computer aided engineering design

Step 1: Define optimization problem

Multi-objective optimization problem for the proposed CPP was proposed to enhance two mentioned quality responses, simultaneously.

Step 2: Define design variables and objective functions

The length of first lever, distance between two levers and thickness of compliant joints were determined as input variables. The quality characteristics were considered, including a large output y-axis displacement and a high safety factor.

Step 3: Create 3D model and simulations

A 3D model is designed by using finite element method (FEM). During the analysis, the relationship between stress and strain was calculated as follows:

$$\sigma = E\varepsilon, \quad (11)$$

where σ , E , ε are stress, Young's modulus and strain, respectively.

Step 4: Test initial quality characteristics by FEM simulation

Initial quality characteristics were checked many times in order to limit suitable upper and lower bounds of design variables and two quality output responses before building design of experiments.

Step 5: Build design of experiments and collect data by integrating of RSM and FEM

The numerical experimentations were collected based on RSM and FEM. Firstly, based on a initial checked 3D model was designed and checked in the FEM in the

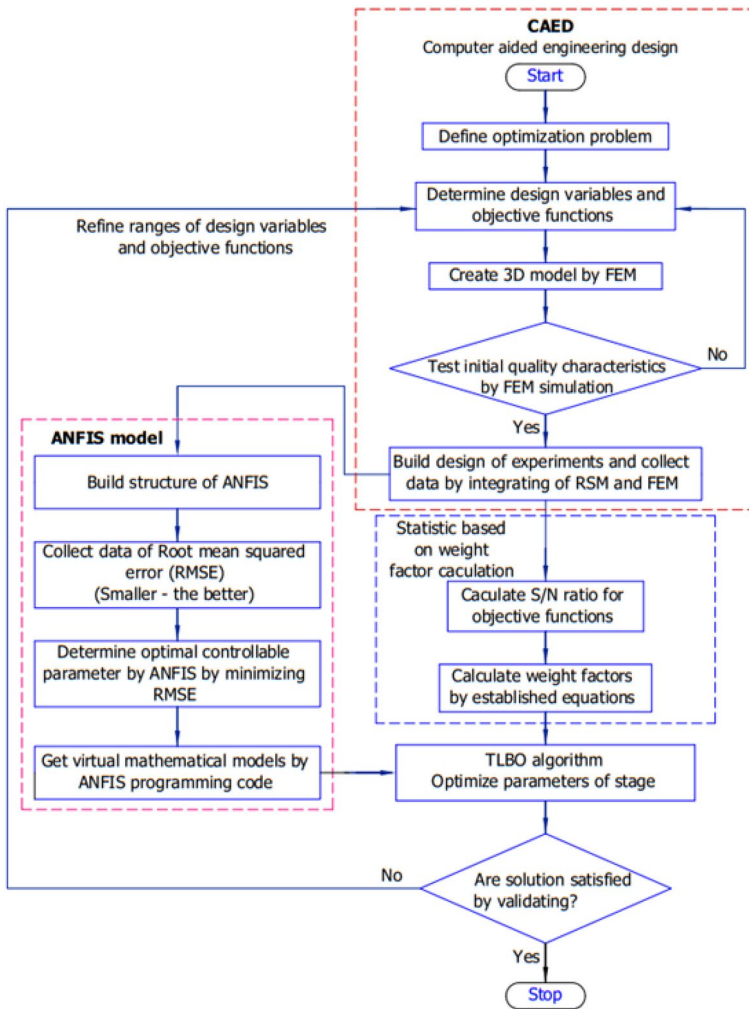


Fig. 8 Flowchart of multi-criteria optimization for compliant positioning platform

step 3 and 4. Then, the number of numerical experiments were established via using the central composite design integrated with RSM. Later on, the estimated results for the quality responses were retrieved. The number of necessary experiments was determined by the following equation:

$$N = 2^{(k-f)} + 2k + n_c, \tag{12}$$

where N was the total of the design points, k was the number of design variables, f was the factorial number ($f=0$), and $n_c = 1$ was the number of replicates at the central point of the design space. In this research, $k=4$, the factorial number for this circumstance of four design variables is $f=0$. Replacing these values into Eq. (12), overall 25 design points are needed for the design of experiments.

Phase 2: define the weight factor

The two quality responses were conflicted. In addition, they had different important weights. Therefore, each objective function can established a WF. So far, the WF was defined according to a design experiences and specialized knowledge. So, in order to calculate the WF more accurately, we followed the methods of Dao et al. (2017a, b) to compute the WF for each response. Details about the WF computing equations, the readers can refer to Dao et al. (2017a, b). Every response function is normalized in the range [0, 1]. The WF is computed as follows:

(1) Compute signal-to-noise ratio (S/N)

The *S/N* ratio is established by the TM and it illustrates a better ability corresponding to a larger *S/N* ratio value. The-larger-the-better is utilized for two reponses in this study, which was expressed by:

$$\eta = -10 \log \left(\frac{1}{n} \sum_{i=1}^n \frac{1}{y_i^2} \right), \quad (13)$$

where *n* is the number of repetitions of experiment *ith*, *y* is the quality feature

(2) Normalize the *S/N* ratio

The normalized *S/N* ratios of each grade of each response function are computed by:

$$z_i = \frac{\eta_j - \min \eta_j}{\max \eta_j - \min \eta_j}, \quad (14)$$

where η_i illustrates the *S/N* value, $\max \eta_i$ and $\min \eta_i$ are the highest and smallest values of η_i , respectively, z_i is the normalized value of *S/N* for the experiment *ith* of response function ($j = 1, 2, \dots, k$), *k* is the number of response functions.

(3) Compute the mean value of normalized *S/N* ratios

The mean value of normalized *S/N* ratios at every grade for design variables were calculated for response functions. The *S/N* ratio values are normalized and the mean value of normalized *S/N* ratios can be defined as follows:

$$a_{Li} = \frac{1}{N_{Li}} \sum_i^m z_{ij}, \quad (15)$$

where N_{Lji} is number of repetition of grade *ith*. z_{ij} is the value of *S/N* ratio of grade *ith* of response function *jth*. a_{Li} is the mean value of *S/N* ratio of grade *ith* of every design variable of every response function.

(4) Calculate the range of each input variable

The range of the every grade of every input variable was defined as following equation:

$$r_{ij} = \max\{z_{i,j,1}, z_{i,j,2}, \dots, z_{i,j,m}\} - \min\{z_{i,j,1}, z_{i,j,2}, \dots, z_{i,j,m}\}, \tag{16}$$

where r_{ij} is the range (max–min) of the S/N value for every grade of every parameter, $j = 1, 2, \dots, q$, q is the number of input variables, $m = 1, 2, \dots, l$, l is the number of experimental grade of every input variable.

(5) Define the weight factor

The weight factor (WF) is computed by:

$$w_i = \frac{\sum_{j=1}^q r_{ij}}{\sum_{i=1}^{m_{OF}} \sum_{j=1}^q r_{ij}}, \tag{17}$$

where w_i ($w_i \geq 0$) is the WF of each response function i th.
 m_{OF} is the number of response functions.

Generally, total of weight factor for total response functions are amounting to 1 and the equation is expressed by:

$$\sum_{i=1}^{m_{OF}} w_i = 1, \tag{18}$$

Phase 3: adaptive neuro-fuzzy inference system

ANFIS is a multi-layer feed-forward network which utilizes integration of neural network and fuzzy reasoning rules based on the merits of both fuzzy logic and artificial neural networks. Fuzzy logic is based on the consideration that people do determinations according to unaccurate and non-numerical information (Tsai et al. 2015; Bhattacharyya et al. 2015, Chau et al. 2018). The implementation of ANFIS architecture based on a first order Sugeno fuzzy inference system is more effective and rapid than the traditional methods as the error back propagation algorithm. In this paper, the fuzzy if–then rules can be described as:

$$\text{if } x_1 \text{ is } A_1 \text{ and } x_2 \text{ is } A_2, \text{ then } y = p \times x_1 + q \times x_2 + r \tag{19}$$

where x_1 and x_2 are inputs corresponding A_1 and A_2 term set, y is output, p , q , r are constant.

The architecture of a representative ANFIS comprises of five layers, which conduct various operations in the ANFIS and are detailed below.

- (1) Layer 1: This layer conducts a fuzzification to generate the membership grades of the inputs. The outputs of this layer are identified by:

$$M_1^i = \mu A_i(x) \quad (20)$$

where x is input to node i , and A_i is linguistic label associated with this node function. M_1^i is the membership function of A_i .

- (2) Layer 2: Each node in this layer is fixed node, marked by a circle and labeled Π . Each node output can be expressed by:

$$w_i = \mu A_i(x) \times \mu A_i(y) \dots i = 1, 2, 3, \dots, N \quad (21)$$

where w_i is the firing strength of a rule.

- (3) Layer 3: Each node in this layer is fixed node, marked by a circle and labeled N . The node function is normalized the firing strength by computing the ratio of the i th node firing strength to the sum of all rules' firing strength.

$$\bar{w} = \frac{w_i}{w_1 + w_2 + w_3, \dots, +w_n}, i = 1, 2, 3, \dots, N \quad (22)$$

where \bar{w} is the normalized firing strength of rules.

- (4) Layer 4: Each node in this layer is an adaptive node, symbolized by a square. Each node i is expressed by:

$$M_1^i = \bar{w}_i f_i(px + qy, \dots, r), i = 1, 2, 3, \dots, N \quad (23)$$

where \bar{w}_i is the output of layer 3 and p, q, r are the parameters set, referred to as the consequent parameters.

- (5) Layer 5: Each node in this layer is a fixed node marked Σ , which calculates the total output as the sum of all incoming signals by:

$$M_5^i = \sum_i \bar{w}_i f_i \frac{\sum_i w_i f_i}{w_i} \quad (24)$$

The hybrid learning algorithm of the ANFIS integrate the gradient algorithm and the least squares method in order to update the parameters. Learning and modifying these adjustable parameters is the two-step process, which comprises a forward pass and a backward pass. In the forward pass, the premise parameters are hold fixed, node outputs go forward to layer 4. The consequent parameters are defined by the least squares.

Moreover, the four design parameters, including length of first lever, distance between two levers and thickness of compliant joints, t, h, b, k contributed the highest impact on two quality characteristics, comprising the y-axis displacement and the safety factor. Therefore, the architecture of ANFIS for the CPP is expanded, as depicted shown in Fig. 9.

As depicted in Fig. 9, five network layers are utilized by ANFIS to conduct the following fuzzy inference steps: (1) input fuzzification, (2) fuzzy set database construction, (3) fuzzy rule base construction, (4) decision making, and (5) output defuzzification.

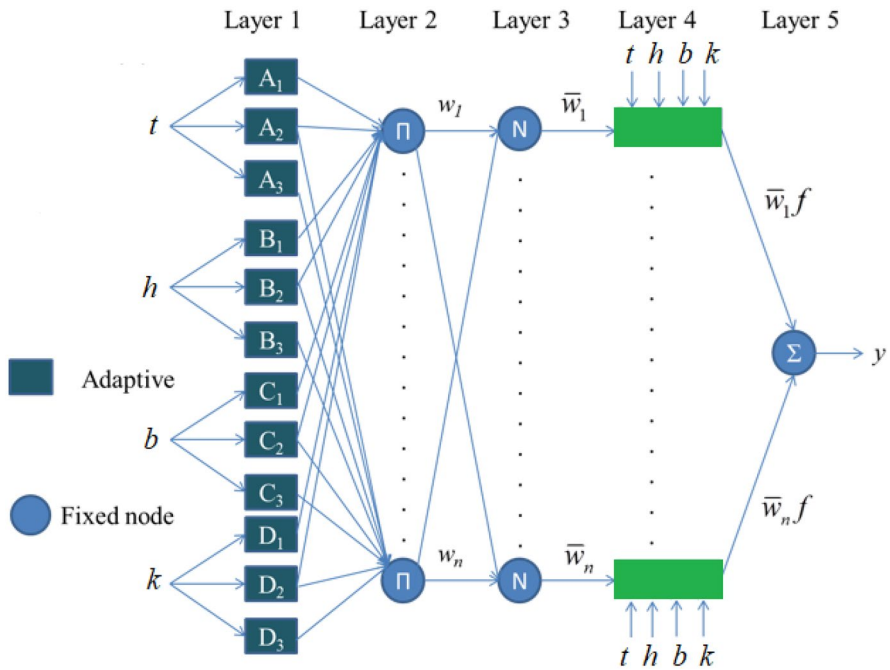


Fig. 9 Proposed ANFIS for the compliant positioning platform

Phase 4: TLBO algorithm

Based on the established surrogate models for objective functions by the improved ANFIS, the optimization process was implemented by TLBO algorithm. Operation principle of this algorithm mimics the teaching-learning ability of the trainer and learners in a classroom. The expected learning outcome of TLBO was the marks results of students depended on the ability of trainer. It forecasted that a good quality student is because of a perfect training based on an excellent trainer. Moreover, besides learning from the trainer, the students can study other intellectuality from various members in class to enhance their marks. Courses were regarded as design variables and the student's results were same the fitness value of the optimal process. The algorithm includes two phases: (1) trainer phase where candidates were distributed at random over the search space and the best solution was determined and (2) student phase where solutions tried to get new intellectuality from communicating with various learners. Details of the TLBO could be found in Rao and Patel (2013), Rao et al. (2011, 2012), Kumar and Singh (2018), Tawhid and Savsani (2018) and Singh et al. (2018).

Table 4 Design of number of experiments and computational results

No.	t (mm)	h (mm)	b (mm)	k (mm)	y_1 (mm)	y_2
1	1.0	20.75	50.5	0.705	1.8324	2.3562
2	0.9	20.75	50.5	0.705	1.8382	2.3633
3	1.1	20.75	50.5	0.705	1.8237	2.3359
4	1.0	19.0	50.5	0.705	1.5594	2.3628
5	1.0	22.5	50.5	0.705	1.7083	2.2432
6	1.0	20.75	48.0	0.705	1.949	2.3107
7	1.0	20.75	53.0	0.705	1.7089	2.3064
8	1.0	20.75	50.5	0.670	1.8473	2.4058
9	1.0	20.75	50.5	0.74	1.828	2.3224
10	0.9	19.0	48.0	0.670	1.5241	2.3751
11	1.1	19.0	48.0	0.670	1.5599	2.3374
12	0.9	22.5	48.0	0.670	1.7716	2.2326
13	1.1	22.5	48.0	0.670	1.7351	2.2422
14	0.9	19.0	53.0	0.670	1.5141	2.4065
15	1.1	19.0	53.0	0.670	1.5624	2.3441
16	0.9	22.5	53.0	0.670	1.7048	2.2387
17	1.1	22.5	53.0	0.670	1.6972	2.2104
18	0.9	19.0	48.0	0.740	1.5264	2.2961
19	1.1	19.0	48.0	0.740	1.6359	2.2674
20	0.9	22.5	48.0	0.740	1.731	2.1849
21	1.1	22.5	48.0	0.740	1.7701	2.1933
22	0.9	19.0	53.0	0.740	1.5835	2.2922
23	1.1	19.0	53.0	0.740	1.5844	2.2415
24	0.9	22.5	53.0	0.740	1.6912	2.1562
25	1.1	22.5	53.0	0.740	1.6867	2.1446

6 Results and discussion

6.1 Collection of numerical data

First of all, a 3D model of the CPP was built via using FEM. A model was chosen for analysis and optimization later. Because there were four design variables, the number of experiments were 25, which was generated by the central composite design through the RSM. Later on, the boundary conditions and input displacement were assigned for the proposed platform. Eventually, by integrating of FEM and RSM, the values of two quality characteristics were retrieved, as depicted in Table 4.

6.2 Calculation of weight factor

Later on, the experimental data were conveyed to the S/N ratios utilizing Eq. (13), as shown in Table 5. The S/N ratios were then normalized utilizing Eq. (14), as

Table 5 The values of S/N ratios

No.	Safety factor (η_1)	Displacement (η_2)	No.	Safety factor (η_1)	Displacement (η_2)
1	5.26040566	7.444243	14	3.60309119	7.6277173
2	5.28785524	7.4703771	15	3.87584461	7.3995227
3	5.21906796	7.3690849	16	4.63346873	6.999918
4	3.8591506	7.4685392	17	4.59466046	6.8894174
5	4.65128282	7.0173599	18	3.67336715	7.219816
6	5.79623678	7.2748713	19	4.27513505	7.1105628
7	4.654333	7.2586926	20	4.76594136	6.7886313
8	5.3307486	7.6251904	21	4.95995604	6.8219608
9	5.23952383	7.3187405	22	3.99236135	7.2050502
10	3.66026926	7.513638	23	3.99729667	7.0107749
11	3.86193516	7.3746608	24	4.5638994	6.6737808
12	4.96731343	6.9762184	25	4.5407569	6.626926
13	4.7864902	7.013487			

Table 6 The normalized S/N ratios (z_i)

No.	Z_1 of η_1	Z_2 of η_2	No.	Z_1 of η_1	Z_2 of η_2
1	0.7557	0.8167	14	0.0000	1.0000
2	0.7682	0.8428	15	0.1244	0.7720
3	0.7368	0.7416	16	0.4698	0.3727
4	0.1168	0.8409	17	0.4521	0.2623
5	0.4779	0.3901	18	0.0320	0.5924
6	1.0000	0.6474	19	0.3064	0.4833
7	0.4793	0.6313	20	0.5302	0.1616
8	0.7878	0.9975	21	0.6187	0.1949
9	0.7462	0.6913	22	0.1775	0.5777
10	0.0261	0.8860	23	0.1797	0.3835
11	0.1180	0.7471	24	0.4381	0.0468
12	0.6220	0.3490	25	0.4275	0.0000
13	0.5396	0.3863			

illustrated in Table 6. In this Table, the normalized S/N ratios for safety factor (η_1) and the displacement (η_2) were Z_1 , and Z_2 , respectively. Utilizing the Eqs. (16) and 17, the WF for the displacement and safety factor were calculated, as shown in Tables 7 and 8, respectively. The WF of the safety factor was 0.4416 and the WF of displacement was 0.5584. Sum of two WFs were equal to one. Generally, the WF for each characteristic was assigned 0.5 but this value was not correct. This would lead unaccurate optimized solution. As a result, this paper suggested an effective approach to determine the WFs.

Table 7 The weight factor for the safety factor

Level	The mean value of normalized <i>S/N</i> ratios of each level			
	<i>A</i>	<i>B</i>	<i>C</i>	<i>D</i>
Level 1	0.3404	0.1201	0.4215	0.3489
Level 2	0.6234	0.7534	0.6270	0.6192
Level 3	0.3893	0.5085	0.3054	0.3840
Range r_{ij}	0.2829	0.6333	0.3217	0.2704
Weight factor for the safety factor: $w_1 = 0.4416$				

Table 8 The weight factor for the y-axis displacement

Level	The mean value of normalized <i>S/N</i> ratios of each level			
	<i>A</i>	<i>B</i>	<i>C</i>	<i>D</i>
Level 1	0.5366	0.6981	0.4942	0.6414
Level 2	0.7165	0.7669	0.7601	0.7015
Level 3	0.3893	0.2404	0.4496	0.3479
Range r_{ij}	0.3272	0.5265	0.3105	0.3536
Weight factor for the displacement: $w_2 = 0.5584$				

6.3 Establishment of ANFIS model

ANFIS is same to a good black box or surrogate model where maps multiple inputs and outputs. In this paper, four design variables affected significantly to the two quality responses and the mathematical equations between them were complicated to set up. Therefore, ANFIS was an suitable tool for this research.

Basically, the controllable parameters of ANFIS could be used as default but some were suitable and others were not appropriate for the proposed CPP. For example, the MFs have a few common types such as trimf, trapmf, gbellmf, gaussmf, sigmf, and pimf. This simulation takes a lot of time but the retrieving solutions may be not reliable. To suppress this effect and make a good result, the suitable MFs were determined by optimizing the *RMSE* which was used as a performance criterion of ANFIS structure. Moreover, the ANFIS algorithm also depends on the training method, the number of MFs, and the type of output MFs.

To do an optimization for the *RMSE*, the controllable parameters of proposed ANFIS were identified and divided into their levels based on the specialized intellectuality and design engineer’s experiences, as depicted in Table 9. The number of input MFs were divided into levels as 3, 4, 5, 6 MFs. Moreover, the trimf, trapmf, gbellmf, and gaussmf were used as levels of the types of input MFs. The optimal learning method for the proposed ANFIS structure was divided into as hybrid learning procedure and backpropagation. Final sensitive factor of ANFIS structure was the types of output MFs that separated into constant or linear value. It was difficult to say which ones were the better for the ANFIS algorithm. As a result, an

Table 9 The levels of controllable factors for the *RMSE*

Factors	Symbol	Level 1	Level 2	Level 3	Level 4
Number of input MFs	<i>A</i>	3	4	5	6
Types of input MFs	<i>B</i>	rimf	trapmf	gbellmf	gaussmf
Optimal training method	<i>C</i>	Hybrid	Backpropa		
Types of output MFs	<i>D</i>	Constant	Linear		

Table 10 Orthogonal array design L_{16} for the *RMSE* of the safety factor

No.	<i>A</i>	<i>B</i>	<i>C</i>	<i>D</i>	<i>RMSE</i> for y_1	<i>S/N</i> ratios for y_1 (dB)
1	3	trimf	Hybrid	Constant	1.6991E-06	115.3956
2	3	trapmf	Hybrid	Constant	1.6991E-06	115.3956
3	3	gbellmf	Backproba	Linear	0.97701	0.20202
4	3	gaussmf	Backproba	Linear	0.96576	0.302616
5	4	trimf	Hybrid	Linear	1.8333E-07	134.7353
6	4	trapmf	Hybrid	Linear	1.8128E-07	134.833
7	4	gbellmf	Backproba	Constant	1.6881	-4.54796
8	4	gaussmf	Backproba	Constant	1.6878	-4.54642
9	5	trimf	Backproba	Constant	1.6832	-4.52271
10	5	trapmf	Backproba	Constant	1.6831	-4.5222
11	5	gbellmf	Hybrid	Linear	7.1854E-06	102.871
12	5	gaussmf	Hybrid	Linear	2.4086E-06	112.3647
13	6	trimf	Backproba	Linear	1.097	-0.80413
14	6	trapmf	Backproba	Linear	1.0906	-0.75331
15	6	gbellmf	Hybrid	Constant	7.1147E-06	102.9569
16	6	gaussmf	Hybrid	Constant	6.5819E-06	103.633

appropriate approach to determine these sensitive parameters of ANFIS was based on statistics and the TM.

Based on four parameters and their levels, an orthogonal array design L_{16} (4^2 & 2^2) was made to construct the 16 different training experiments for the ANFIS. The data of the y-axis displacement in the Table 4 would be conducted as training data and these data were trained in the ANFIS algorithm. And then, the *RMSE* values were determined and *S/N* ratios were computed using the TM. The results of *RMSE* and *S/N* ratios for the safety factor were calculated using the TM, as shown in Table 10.

To identify the optimal *RMSE* of the safety factor for the further ANFIS structure, the mean response of *S/N* ratios and main diagram of effects of each parameters were solved. From the results in Table 11 and Fig. 10, the optimal parameters were determined at the number of input MFs of 4, trapmf, hybrid learning method, and linear output MFs. The results also found that the optimal *S/N* ratio of *RMSE* is 134.833, as given in Table 12. This value was largest value compared with the values in Table 10. It proved that a larger *S/N* ratio is corresponding to a better solution.

Table 11 Mean response for *S/N* ratios for the *RMSE* of the safety factor

Level	A	B	C	D
1	0.48569	0.66339	1.35907	0.84278
2	0.84398	0.66628	0.00000	0.51630
3	0.84158	0.69343		
4	0.54690	0.69505		
Delta	0.35828	0.03166	1.35907	0.32648
Rank	2	4	1	3

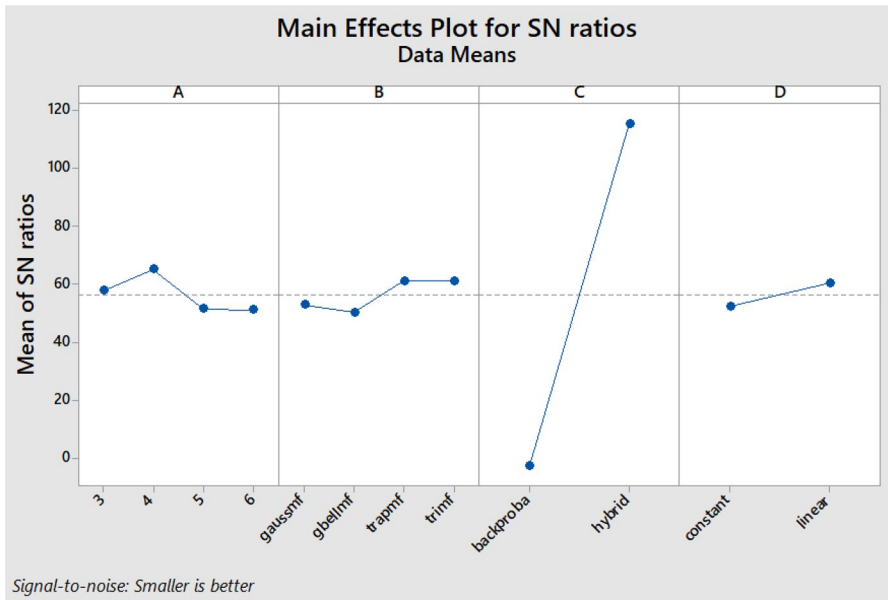


Fig. 10 Response diagram of the *RSME* of the safety factor

Table 12 Prediction of optimal *RMSE* of of the safety factor

Settings				Optimal <i>S/N</i> ratio (dB) of <i>RMSE</i>
A	B	C	D	
4	trapmf	Hybrid	Linear	134.833

Similarly, the optimizing process for the *RMSE* of displacement was carried out. The *RMSE* results for the displacement were given in Table 13. Based on the mean response for *S/N* ratios for the *RMSE* of safety factor and main diagram of effect in Table 14 and Fig. 11, the optimal controllable parameters for further ANFIS structure were found at the number of input MFs of 4, the trapmf, hybrid learning method, and linear output MFs. Also in Table 15, the optimal results

Table 13 Orthogonal array design L_{16} for the *RMSE* of the displacement

No.	A	B	C	D	<i>RMSE</i> of y_2	<i>S/N</i> ratios for y_2 (dB)
1	3	trimf	Hybrid	Constant	2.29E-06	112.8109
2	3	trapmf	Hybrid	Constant	2.29E-06	112.8109
3	3	gbellmf	Backproba	Linear	1.5641	- 3.88529
4	3	gaussmf	Backproba	Linear	1.5527	- 3.82175
5	4	trimf	Hybrid	Linear	2.3E-07	132.7613
6	4	trapmf	Hybrid	Linear	2.48E-07	132.1082
7	4	gbellmf	Backproba	Constant	2.2768	- 7.1465
8	4	gaussmf	Backproba	Constant	2.2766	- 7.14573
9	5	trimf	Backproba	Constant	2.2721	- 7.12855
10	5	trapmf	Backproba	Constant	2.272	- 7.12817
11	5	gbellmf	Hybrid	Linear	1.02E-05	99.82715
12	5	gaussmf	Hybrid	Linear	2.73E-06	111.2694
13	6	trimf	Backproba	Linear	1.6419	- 4.30693
14	6	trapmf	Backproba	Linear	1.6341	- 4.26557
15	6	gbellmf	Hybrid	Constant	9.25E-06	100.6794
16	6	gaussmf	Hybrid	Constant	8.63E-06	101.2775

Table 14 Mean response for *S/N* ratios for the *RMSE* of the displacement

Level	A	B	C	D
1	0.77920	0.95733	1.93629	1.13719
2	1.13835	0.96023	0.00000	0.79910
3	1.13603	0.97653		
4	0.81900	0.97850		
Delta	0.35915	0.02117	1.93628	0.33809
Rank	2	4	1	3

depicted that the optimal *RMSE* is approximately 132.1082 being higher than the *S/N* ratio values in Table 13. This means that the optimal *RMSE* is accepted.

The ANFIS regularly uses the typical membership functions such as Gaussian, sigmoidal, triangular, trapezoidal, and bell types. Therefore, it is difficult to seek the suitable appropriate MFs. In this study, based on the results on Tables 9, 10, 11, 12, 13, 14 and 15, the trapezoidal was suitable for an improved ANFIS structure for modeling the CPP. The trapezoidal membership function was expressed by:

$$\mu_A(x, a, l, r, b) = \begin{cases} \frac{(x-a)}{(l-a)} & a \leq x \leq l \\ 1 & l < x < r \\ \frac{(x-b)}{(r-b)} & r \leq x \leq b \end{cases}, \tag{25}$$

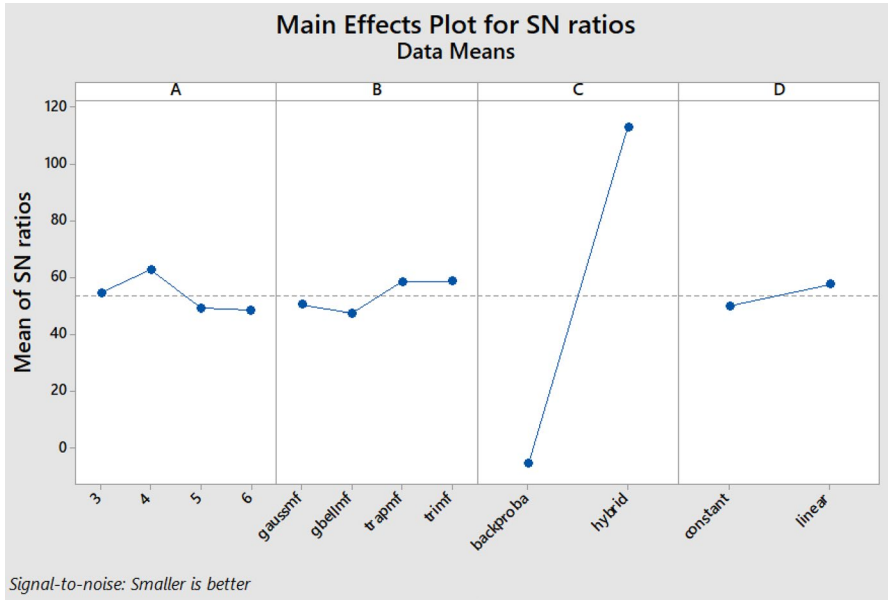


Fig. 11 Response diagram of the *RSME* of the *y*-axis displacement

Table 15 Prediction of optimal *RMSE* of the *y*-axis displacement

Settings				Optimal <i>S/N</i> ratio (dB) of <i>RMSE</i>
A	B	C	D	
4	trapmf	Hybrid	Linear	132.1082

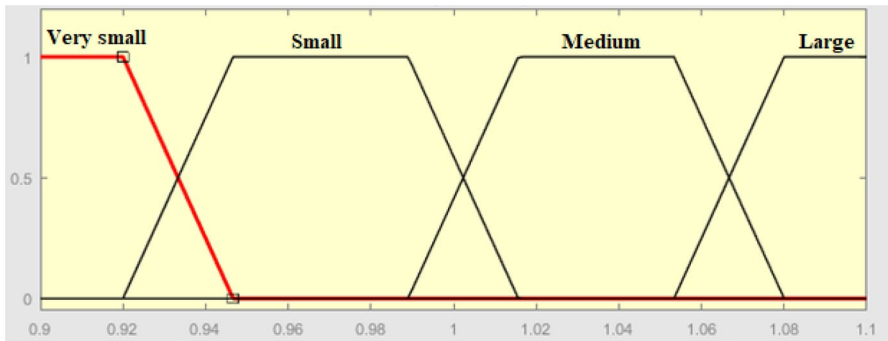


Fig. 12 Shape of trapezoidal membership function

where μ_A depicts the MFs of the fuzzy set; a, b, l and r represent parameters; and x is variable. The shape of trapezoidal MFs were given, as illustrated in Fig. 12.

After the suitable controllable parameters of ANFIS were determined based on the TM, the improved ANFIS structure was generated, as illustrated in Fig. 13.

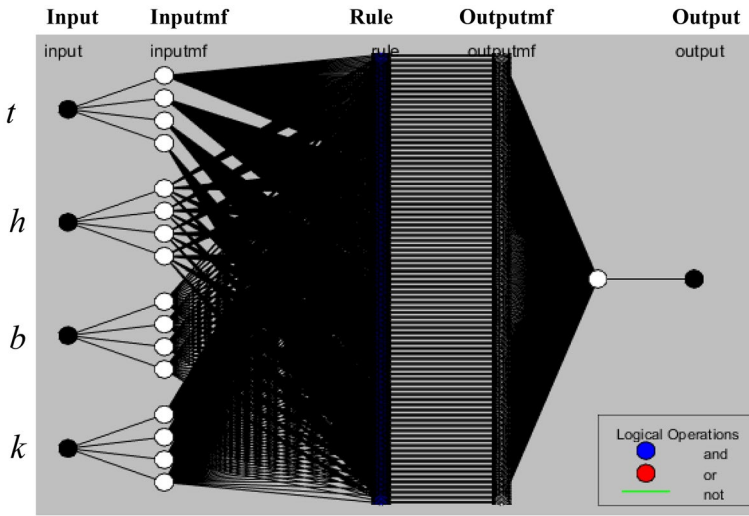


Fig. 13 Model for improved ANFIS structure

Table 16 ANFIS parameters

Number of nodes	551
Number of linear parameters	1280
Number of nonlinear parameters	48
Total number of parameters	1328
Number of training data pairs	25
Number of testing data pairs	0
Number of fuzzy rules	256

The number of linear parameters were 1280, as seen in this Table 16. By contrast, the number of nonlinear parameters were 48. If an analytical approach was utilized, many parameters can not determine accurately. In conclusion, ANFIS was the suitable method to apply for the suggested CPP.

6.4 Optimal results

After gaining the WFs and the surrogate models for two objective functions, the TLBO was utilized to optimize the CPP. The optimization process was conducted utilizing Matlab 2017. The initial parameters including population size of 30 as well as tolerance of 10^{-6} were utilized for the TLBO. The optimized results were produced at the generation of 79. The optimization input variables were detected at $x_{val} = [0.67 \ 0.9 \ 19 \ 53]$ and $f_{val} = -2.01241668736275$. The optimized solutions were corresponding to $t = 0.9$ mm, $h = 19$ mm, $b = 53$ mm, $k = 0.67$ mm, $y_1 = 1.514097$ and $y_2 = 2.406501242$ mm.

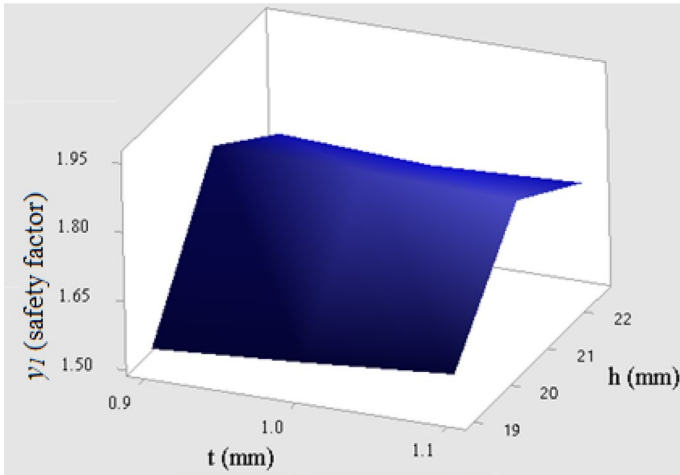


Fig. 14 Effect diagram of t and h on the safety factor

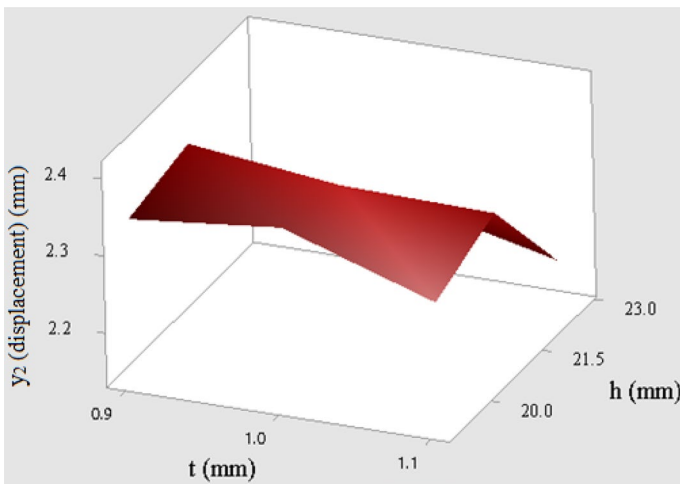


Fig. 15 Effect diagram of t and h on the output displacement

6.5 Sensitivity analysis

Statistical technique was utilized to identify the effect grade of variables on the quality responses. As seen in Figs. 14 and 15, factor t illustrated that in the range from 0.9 to 1 mm, this parameter affected to y_1 and y_2 in increasing gradually, but in the range from 1 to 1.1 m, it caused gradually to y_1 and y_2 a reduction. Moreover, factor h showed that in the range from 19 to 20.75 mm, it affected a sharp rise to y_1 and caused a slight rise to y_2 , however, from 20.75 to 22.5 mm, there was a gradual reduce to y_1 and a sharp reduce to y_2 .

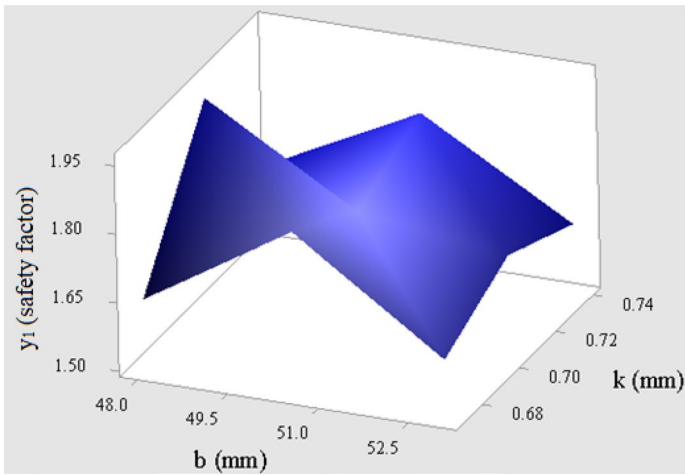


Fig. 16 Effect diagram of b and k on the safety factor

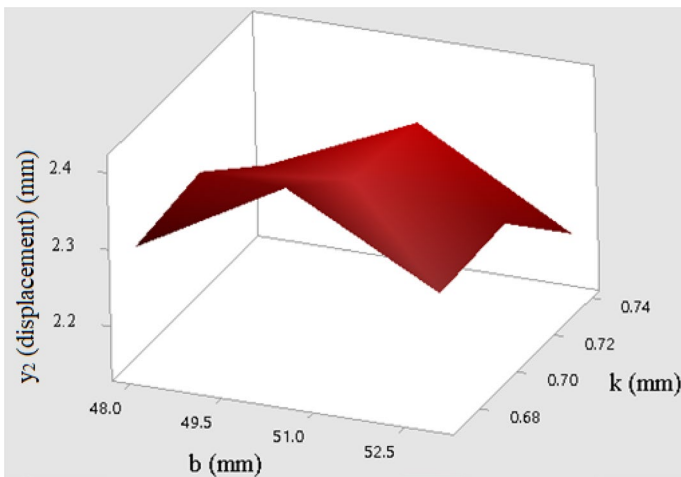


Fig. 17 Effect diagram of b and k on the displacement

As drawn in Figs. 16 and 17, factor b indicated that in the range from 48 to 50.5 mm, it affected a gradual rise to y_1 and y_2 , but, from 50.5 to 53 mm, there was a both gradual reduce to y_1 and y_2 . Eventually, factor D illustrated that in the range from 0.67 to 0.705 mm, it affected gradual rise to y_1 and caused a slight rise to y_2 , however, from 0.6 to 0.7 mm, there was a both gradual decrease to y_1 and y_2 .

In conclusion, overall effects of design variables were showed, as in Fig. 18. It reveals an increase and decrease range in each factor. Therefore, the designers could control the factors so as to obtain a best structure for the proposed CPP.

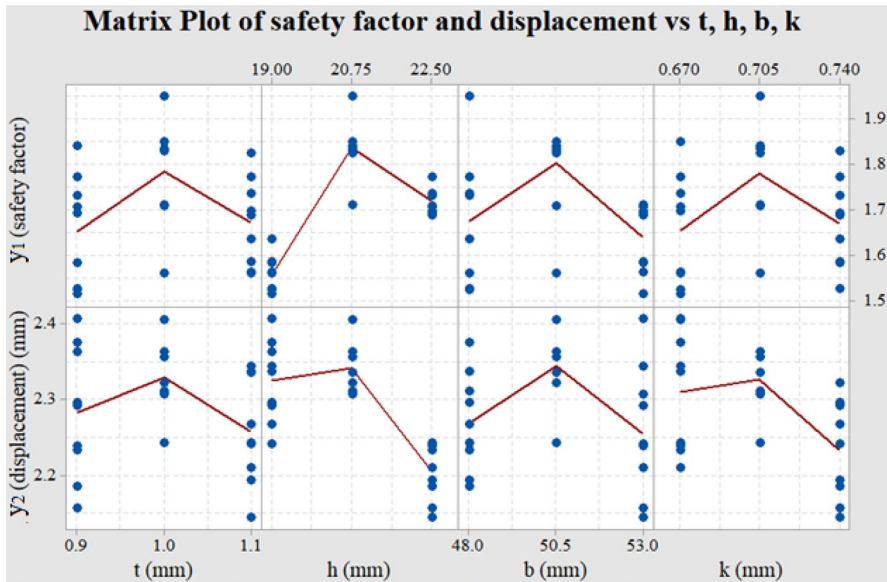


Fig. 18 Sensitivity diagram of the parameters on the responses

7 Verifications

To verify the optimized characteristics of the suggested CPP, the numerical simulations and experiments were carried out. Using the optimal parameters ($t=0.9$ mm, $h=19$ mm, $b=53$ mm, $k=0.67$ mm), a 3D model was designed in Inventor software and imported into ANSYS software in order to conduct simulations. The meshes of flexure hinges were refined to enhance the accuracy of analysis quality. And then, using the optimal design variables, the prototype of the CPP platform was fabricated by wire electrical discharged machining. As shown in Fig. 19, the experiments were implemented as follows: an input displacement was driven translational screw mechanism measured displacement by Digital dial indicator 1 (High precision 0.001 mm, 543-390B, Mitutoyo Japan). In addition, output displacement was measured by Digital dial indicator 2 (High precision 0.001 mm, 543-390B, Mitutoyo Japan) and Digital dial indicator mounted Magnetic base (Mitutoyo Japan).

As seen in Table 17, the maximum of the y-axis probed deformation was 2.427 mm and the minimum of safety factor was 1.526. Based on the FEA result, the error between predicted result of optimal result is small: the error of safety factor is 0.786%. In addition, Table 17 illustrates that an error between optimal result and FEA test is also small: error of the probed displacement between optimal result and FEA result is 0.824% and between experimental result and FEA result is 7.581%. It means that there is a good agreement between the forecasted values and validations. Meanwhile, there were also some sources such as meshing, fabricating and material errors that could reduce these errors. Therefore, the suggested integrated optimal algorithm was reliable and effectual to optimize the CPP. Therefore, the proposed hybrid approach of

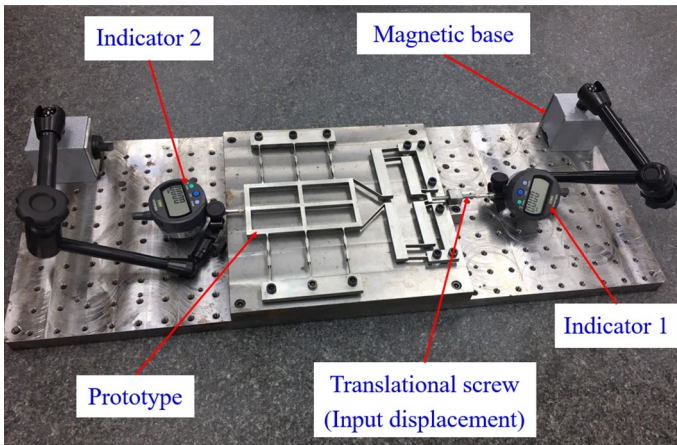


Fig. 19 Experimental installation for the prototype

Table 17 Comparison among the optimization, FEA, and experimental results

Characteristics	Optimization result	FEA result	Experimental result	Error (%) (between optimization and FEA results)	Error (%) (between FEA and experimental results)
y_1 (mm)	2.406	2.427	2.243	0.824	7.581
y_2	1.514	1.526	–	0.786	–

FEM-based RSM, TM, improved ANFIS, and TLBO is enough reliable to search the optimal solution in this study. The experimental process was conducted 10 times and computed average values for experimental results.

The strong abilities of the positioning platform are summarized by: it allowed to gain working travel approximately 2406 μm , a displacement amplification ratio of more than 18 times. Compared with some previous researches, the proposed platform had a better working stroke. In conclusion, the results demonstrated that two referred regards are precise as the supposed theory. It can conclude the highlight performances as follows: (a) proposed platform allowed to achieve high displacement while safety factor is also more than 1.5 in order to ensure the platform working in the elastic condition and (b) the output displacement of the positioning platform is more than 18 times the input displacement. Figure 20 indicates relationship between input displacement and output displacement for FEA results and experiment results, respectively.

8 Conclusions

This paper proposed an efficient hybrid optimization approach for the compliant positioning platform. The CPP was expected to locate the sample during nanoindentation tester. The proposed CPP was integrated the four-lever mechanism amplifier and beetle-like structure. The platform imitated the biomechanical

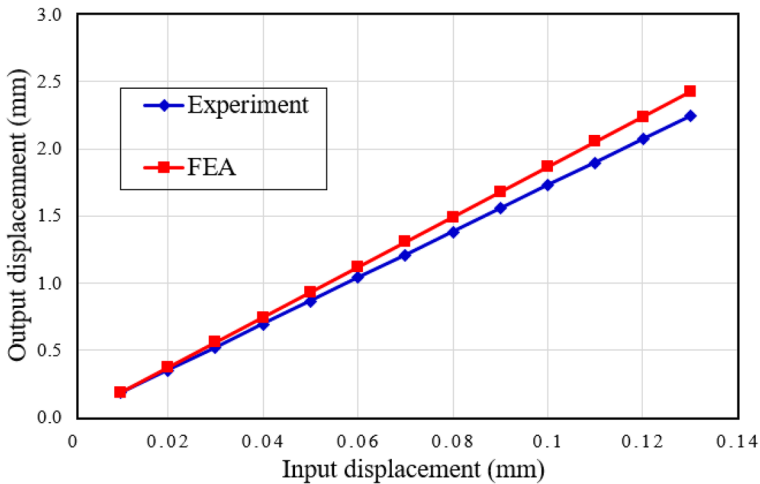


Fig. 20 Relationship plot of the input displacement vs the output displacement

behavior of beetle in order to reach a linear displacement and reduce parasitic motion.

To enhance the output displacement and safety factor simultaneously, the main geometric parameters of proposed CPP were optimized by an integration of the RSM, FEM, TM, improved ANFIS and TLBO. The *RMSE* was optimized by the TM to find suitable controllable parameters for the ANFIS structure. And then, the weight factor of both responses were calculated by establishing the sets of statistical-based equations. The results found that the WFs of safety factor and displacement are 0.4416 (44.16%) and 0.5584 (55.84%), respectively. The WF's values were assigned into the TLBO algorithm to conduct the multi-criteria optimal trouble. The sensitivity analysis as well as ANOVA were conducted to define the effects and significant contributions of design variables on the two quality characteristics.

The results illustrated that the optimal parameters were found at $t=0.9$ mm, $h=19$ mm, $b=53$ mm, $k=0.67$ mm. In addition, the results indicated that the optimal safety factor is 1.5141 and the optimal displacement is approximately 2.4065 mm. Moreover, the results depicted that the errors between the optimal results and the FEA validations for the safety factor and output displacement are 0.786% and 0.824%, respectively. The error between experimental result and the forecasted result was about 7.581%. The proposed hybrid approach is useful and effective to carry out the multi-criteria optimal trouble for complex design.

Acknowledgements The authors are thankful for the financial support from the HCMC University of Technology and Education, Vietnam, under Grant No. T2019-05TD.

Compliance with ethical standards

Conflict of interest The authors declare that they have no conflict of interest.

References

- Álvarez MJ, Ilzarbe L, Viles E, Tanco M (2009) The use of genetic algorithms in response surface methodology. *Qual Technol Quant Manag* 6:295–307. <https://doi.org/10.1080/16843703.2009.11673201>
- Bahloul R, Arfa H, Belhadjalah H (2013) Application of response surface analysis and genetic algorithm for the optimization of single point incremental forming process. *Key Eng Mater* 554–557:1265–1272. <https://doi.org/10.4028/www.scientific.net/KEM.554-557.1265>
- Bhattacharyya S, Basu D, Konar A, Tibarewala DN (2015) Interval type-2 fuzzy logic based multiclass ANFIS algorithm for real-time EEG based movement control of a robot arm. *Robot Auton Syst* 68:104–115. <https://doi.org/10.1016/j.robot.2015.01.007>
- Chau NL, Nguyen MQ, Dao TP, Huang SC, Hsiao TC, Dinh DC, Dang VA (2018) An effective approach of adaptive neuro-fuzzy inference system-integrated teaching learning-based optimization for use in machining optimization of S45C CNC turning. *Optim Eng*. <https://doi.org/10.1007/s11081-018-09418-x>
- Cheng C-H, Wei L-Y (2009) One step-ahead ANFIS time series model for forecasting electricity loads. *Optim Eng* 11:303–317. <https://doi.org/10.1007/s11081-009-9091-5>
- Dao TP, Huang SC (2017a) Compliant thin-walled joint based on zygoptera nonlinear geometry. *J Mech Sci Technol* 31:1293–1303. <https://doi.org/10.1007/s12206-017-0228-8>
- Dao TP, Huang SC (2017b) Design and multi-objective optimization for a broad self-amplified 2-DOF monolithic mechanism. *Sadhana Acad Proc Eng Sci* 42:1527–1542. <https://doi.org/10.1007/s12046-017-0714-9>
- Dao TP, Ho NL, Nguyen TT, Le HG, Thang PT, Pham HT, Do HT, Tran MD, Nguyen TT (2017a) Analysis and optimization of a micro-displacement sensor for compliant microgripper. *Microsyst Technol* 23:5375–5395. <https://doi.org/10.1007/s00542-017-3378-9>
- Dao TP, Huang SC, Thang PT (2017b) Hybrid Taguchi-cuckoo search algorithm for optimization of a compliant focus positioning platform. *Appl Soft Comput J* 57:526–538. <https://doi.org/10.1016/j.asoc.2017.04.038>
- Fung RF, Lin WC (2009) System identification of a novel 6-DOF precision positioning table. *Sens Actuators A Phys* 150:286–295. <https://doi.org/10.1016/j.sna.2009.01.007>
- Hu Z, Lynne KJ, Markondapatnaikuni SP, Delfanian F (2013) Material elastic-plastic property characterization by nanoindentation testing coupled with computer modeling. *Mater Sci Eng, A* 587:268–282. <https://doi.org/10.1016/j.msea.2013.08.071>
- Huang SC, Dao TP (2016a) Design and computational optimization of a flexure-based XY positioning platform using FEA-based response surface methodology. *Int J Precis Eng Manuf* 17:1035–1048. <https://doi.org/10.1007/s12541-016-0126-5>
- Huang SC, Dao TP (2016b) Multi-objective optimal design of a 2-DOF flexure-based mechanism using hybrid approach of grey-taguchi coupled response surface methodology and entropy measurement. *Arab J Sci Eng* 41:5215–5231. <https://doi.org/10.1007/s13369-016-2242-z>
- Kang BH, Wen JTY, Dagalakis NG, Gorman JJ (2005) Analysis and design of parallel mechanisms with flexure joints. *IEEE Trans Robot* 21:1179–1184. <https://doi.org/10.1007/s10773-015-2880-z>
- Kim HY, Ahn DH, Gweon DG (2012) Development of a novel 3-degrees of freedom flexure based positioning system. *Rev Sci Instrum*. <https://doi.org/10.1063/1.4720410>
- Kumar Y, Singh PK (2018) A chaotic teaching learning based optimization algorithm for clustering problems. *Appl Intell* 49(3):1036–1062
- Lai LJ, Zhu ZN (2017) Design, modeling and testing of a novel flexure-based displacement amplification mechanism. *Sens Actuators A Phys* 266:122–129. <https://doi.org/10.1016/j.sna.2017.09.010>
- Le Zhu W, Zhu Z, Guo P, Ju BF (2018) A novel hybrid actuation mechanism based XY nanopositioning stage with totally decoupled kinematics. *Mech Syst Signal Process* 99:747–759. <https://doi.org/10.1016/j.ymsp.2017.07.010>
- Ling M, Cao J, Zeng M, Lin J, Inman DJ (2016) Enhanced mathematical modeling of the displacement amplification ratio for piezoelectric compliant mechanisms. *Smart Mater Struct* 25:1–11. <https://doi.org/10.1088/0964-1726/25/7/075022>
- Ling M, Cao J, Jiang Z, Zeng M, Li Q (2019) Optimal design of a piezo-actuated 2-DOF millimeter-range monolithic flexure mechanism with a pseudo-static model. *Mech Syst Signal Process* 115:120–131

- Linh HN, Dao TP (2018) Optimal design of a compliant microgripper for assemble system of cell phone vibration motor using a hybrid approach of ANFIS and Jaya. Arab J Sci Eng. <https://doi.org/10.1007/s13369-018-3445-2>
- Lu K, Zhang J, Chen W, Jiang J, Chen W (2014) A monolithic microgripper with high efficiency and high accuracy for optical fiber assembly. In: Proceedings of the 2014 9th IEEE conference on industrial electronics and applications, ICIEA, pp 1942–1947. <https://doi.org/10.1109/iciea.2014.6931486>
- Nohava J, Randall NX, Conté N (2009) Novel ultra nanoindentation method with extremely low thermal drift: principle and experimental results. J Mater Res 24:873–882. <https://doi.org/10.1557/jmr.2009.0127>
- O'Brien W (2005) Long-range motion with nanometer precision. Photonics Spectra 39:80–81
- Polit S, Dong J (2011) Development of a high-bandwidth XY nanopositioning stage for high-rate micro-/nanomanufacturing. IEEE/ASME Trans Mechatron 16:724–733. <https://doi.org/10.1109/TMECH.2010.2052107>
- Rao RV, Patel V (2013) Multi-objective optimization of heat exchangers using a modified teaching-learning-based optimization algorithm. Appl Math Model 37:1147–1162. <https://doi.org/10.1016/j.apm.2012.03.043>
- Rao RV, Savsani VJ, Vakharia DP (2011) Teaching–learning-based optimization: a novel method for constrained mechanical design optimization problems. CAD Comput Aided Des 43:303–315. <https://doi.org/10.1016/j.cad.2010.12.015>
- Rao RV, Savsani VJ, Vakharia DP (2012) Teaching–learning-based optimization: an optimization method for continuous non-linear large scale problems. Inf Sci (Ny) 183:1–15. <https://doi.org/10.1016/j.ins.2011.08.006>
- Singh S, Ashok A, Kumar M (2018) Adaptive infinite impulse response system identification using teacher learner based optimization algorithm. Appl Intell 49(5):1785–1802
- Song M-G, Baek H-W, Park N-C, Park K-S, Yoon T, Park Y-P, Lim S-C (2010) Development of small sized actuator with compliant mechanism for optical image stabilization. IEEE Trans Magn. <https://doi.org/10.1109/tmag.2010.2042288>
- Suraj S, Sinha RK, Ghosh S (2016) Jaya based ANFIS for monitoring of two class motor imagery task. IEEE Access 4:9273–9282. <https://doi.org/10.1109/ACCESS.2016.2637401>
- Tawhid MA, Savsani V (2018) A novel multi-objective optimization algorithm based on artificial algae for multi-objective engineering design problems. Appl Intell 48(10):3762–3781
- Thanh-Phong D, Huang S-C, Le Chau N (2018) Robust parameter design for a compliant microgripper based on hybrid Taguchi-differential evolution algorithm. Microsyst Technol 24(3):1461–1477. <https://doi.org/10.1007/s00542-017-3534-2>
- Tsai JT, Chiu KY, Chou JH (2015) Optimal design of SAW gas sensing device by using improved adaptive neuro-fuzzy inference system. IEEE Access 3:420–429. <https://doi.org/10.1109/ACCESS.2015.2427291>
- Wei LY (2016) A hybrid ANFIS model based on empirical mode decomposition for stock time series forecasting. Appl Soft Comput J 42:368–376. <https://doi.org/10.1016/j.asoc.2016.01.027>
- Xiao S, Li Y, Zhao X (2011) Optimal design of a novel micro-gripper with completely parallel movement of gripping arms. In: IEEE conference on robotics, automation and mechatronics, RAM, pp 35–40. <https://doi.org/10.1109/ramech.2011.6070452>
- Xu Q (2014) Design and testing of a novel multi-stroke micropositioning system with variable resolutions. Rev Sci Instrum 85:025002. <https://doi.org/10.1063/1.4866475>
- Xu Q, Li Y (2011) Analytical modeling, optimization and testing of a compound bridge-type compliant displacement amplifier. Mech Mach Theory 46:183–200. <https://doi.org/10.1016/j.mechmachtheory.2010.09.007>
- Yong YK, Aphale SS, Moheimani SOR (2009) Design, identification, and control of a flexure-based XY stage for fast nanoscale positioning. IEEE Trans Nanotechnol 8:46–54. <https://doi.org/10.1109/TNANO.2008.2005829>
- Zukhri Z, Papatungan IV (2013) A hybrid optimization algorithm based on genetic algorithm and ant colony optimization. Int J Artif Intell Appl. <https://doi.org/10.5121/ijaiia.2013.4505>

Affiliations

Minh Phung Dang¹ · Hieu Giang Le¹ · Ngoc Le Chau² · Thanh-Phong Dao^{3,4}

¹ Faculty of Mechanical Engineering, Ho Chi Minh City University of Technology and Education, Ho Chi Minh City, Vietnam

² Faculty of Mechanical Engineering, Industrial University of Ho Chi Minh City, Ho Chi Minh City, Vietnam

³ Division of Computational Mechatronics, Institute for Computational Science, Ton Duc Thang University, Ho Chi Minh City, Vietnam

⁴ Faculty of Electrical and Electronics Engineering, Ton Duc Thang University, Ho Chi Minh City, Vietnam